Photochemical depletion of heavy CO isotopes in the Martian atmosphere

Juan Alday, Alexander Trokhimovskiy, Manish Patel, Anna Fedorova, Franck Lefèvre, Franck Montmessin, James Holmes, Kylash Rajendran, Jon Mason, Kevin Olsen, et al.

Photochemistry on Mars reduces the abundance of heavy isotopes in atmospheric CO and their escape efficiency to space

Juan Alday[a]*, Alexander Trokhimovskiy[b], Manish R. Patel[a], Anna A. Fedorova[b], Franck Lefèvre[c], Franck Montmessin[c], James A. Holmes[a], Kylash Rajendran[a], Jon P. Mason[a], Kevin S. Olsen[a,d], Denis A. Belyaev[b], Oleg Korablev[b], Lucio Baggio[c], Andrey Patrakeev[b] and Alexey Shakun[b].

[a] *School of Physical Sciences, The Open University, Milton Keynes, United Kingdom.*
[b] *Space Research Institute (IKI), Moscow, Russia.*
[c] *LATMOS/CNRS, Guyancourt, France.*
[d] *AOPP, Department of Physics, University of Oxford, Oxford, United Kingdom.*

* Corresponding author. E-mail address: juan.alday@open.ac.uk

Abstract

The atmosphere of Mars is enriched in heavy isotopes with respect to Earth as a result of the escape of the atmosphere to space over billions of years. Estimating the enrichment in heavy isotopes due to atmospheric escape requires a rigorous understanding of all atmospheric processes that contribute to the evolution of isotopic ratios between the lower and upper atmosphere, where escape processes take place. Using a combination of vertical profiles from the Atmospheric Chemistry Suite (ExoMars Trace Gas Orbiter) with the predictions of a photochemical model, we provide evidence for a new process of photochemistry-induced fractionation that depletes the heavy isotopes of C and O in CO. Accounting for this new source of fractionation, we find that only a fraction of ≈12% of the atmosphere needs to have been lost to space through CO photochemical escape to explain the enrichment of $^{13}C/^{12}C$ in CO_2 measured by the Curiosity Rover.

1. Main text

Numerous lines of geomorphological and mineralogical evidence suggest that liquid water was once abundant on Mars' surface (e.g., Baker (2001); Carr & Clow (1981); Head et al. (1999); Murchie et al. (2009)), but it remains unclear what climatic conditions enabled this, or what drove the transition in the climate to the dry, low pressure atmosphere we observe today. Enrichment in the heavy isotopes of several species such as Ar, N and H suggests that atmospheric escape has been an important mechanism shaping the climate and composition of the atmosphere throughout history (e.g., McElroy et al. (1976); Owen (1982); Owen et al. (1988)). Combining measured atmospheric isotope ratios with evolution models allows the estimation of the abundance of species in the atmosphere of early Mars, which demonstrates the value of a thorough understanding of the atmospheric isotope composition (Hu et al., 2015; Hu & Thomas, 2022; Jakosky et al., 2017; Scheller et al., 2021).

Accurate estimations of the long-term evolution of the atmosphere from its isotope composition rely on two important quantities: measurements of the past and present isotopic ratios, and the net escape fractionation factor, which determines the efficiency of the heavy-isotope enrichment as the atmosphere escapes to space (e.g., Krasnopolsky et al. (1998); Yung et al. (1988)). The most accurate measurements of the isotopic composition of C and O in the atmosphere of Mars were made by the Curiosity Rover, which showed an enrichment in the heavy isotopes in CO_2 with respect to Earth-like standards ($^{13}C/^{12}C$ = 1.046 ± 0.004 VPDB and $^{18}O/^{16}O$ = 1.048 ± 0.005 VSMOW, see Methods for definition of

standards), consistent with the hypothesis of substantial atmospheric loss (Mahaffy et al., 2013; Webster et al., 2013). On the other hand, while the fractionation factor of several escape processes of C and O has been estimated before (Fox & Hać, 1999; Fox & Hać, 2010; Hu et al., 2015), the net escape fractionation factor, accounting for all processes from the lower atmosphere to the upper atmosphere as well, remains undetermined.

By applying this methodology to the C isotopes, the density of CO_2 in the atmosphere of early Mars has been estimated (Hu et al., 2015; Jakosky, 2019). The escape of C at present is suggested to occur mostly in the form of hot C produced by a number of different photochemical reactions, such as the direct photodissociation of CO_2 and CO or the dissociative recombination of CO^+ (Cui et al., 2019; Gröller et al., 2014; Lo et al., 2021; McElroy, 1972). Hu et al. (2015) showed that the photodissociation of CO efficiently enriches the atmosphere in ^{13}C as it escapes to space, and whose contribution is an important factor for explaining the current enrichment in ^{13}C in CO_2 measured by the Curiosity Rover. However, whilst CO therefore seems to be an important species for understanding the isotopic evolution of C in the atmosphere of Mars, its present-day isotopic composition has not yet been determined.

Carbon isotopic ratios can also reveal the nature of surface-atmosphere interaction processes and mineral formation. Recently, carbon isotopic measurements by the Curiosity Rover revealed anomalously large depletions in ^{13}C ($^{13}C/^{12}C \approx 0.86$-$0.93$ VPDB) on sedimentary organics potentially associated with a possible paleosurface (House et al., 2022). One of the possible explanations suggested to produce ^{13}C-depleted organic material is the photochemical reduction of CO_2 into formaldehyde (CH_2O) with CO as an intermediate. In this production, the abundance of ^{13}C in CO is suggested to be lower than that in CO_2 as a result of the differential photolysis of $^{12}CO_2$ and $^{13}CO_2$ (Schmidt et al., 2013), transferring its isotopic signature into formaldehyde and other organics that accumulated on the surface of Gale Crater (House et al., 2022). Direct measurements of the $^{13}C/^{12}C$ in CO may therefore provide constraints on whether the photoreduction of CO_2 is the responsible mechanism for the depletion of ^{13}C on the surface organics.

The reactions that determine the abundance of CO in the atmosphere of Mars are the same as the ones controlling the long-term stability of CO_2: the photolysis of CO_2 into CO, and the posterior recombination of CO back into CO_2. The stability of CO_2 in Mars' atmosphere was at first not well understood since the photodissociation of CO_2 molecules ($CO_2 + h\nu \rightarrow CO + O$) is much faster than the recombination of the products ($CO + O + M \rightarrow CO_2 + M$). It was later realised that the stability of CO_2 is instead controlled by catalytic reactions with odd-hydrogen species ($CO + OH \rightarrow CO_2 + H$), which can convert CO into CO_2 at a much faster rate (McElroy & Donahue, 1972; Parkinson & Hunten, 1972). This reaction network not only determines the relative abundances of CO_2 and CO in the atmosphere of Mars, but also controls the relative isotopic fractionation of C and O in these species.

Here, we investigate the isotopic composition of C and O in CO using solar occultation measurements by the Atmospheric Chemistry Suite (ACS) onboard the ExoMars Trace Gas Orbiter (TGO) (Korablev et al., 2018). ACS includes three spectrometers dedicated to investigate the atmosphere using different spectral ranges: the near-infrared channel (NIR), which operates between 0.7-1.7 μm; the mid-infrared channel (MIR) operating between 2.3-4.2 μm; and the thermal infrared channel (TIRVIM), which samples the atmosphere between 0.7-17 μm. In this study, we use observations from the MIR channel, which is dedicated to solar occultation observations. For these observations, the instrument's boresight is pointed towards the Sun as it rises or sets from behind the Mars disk. By making measurements every 2.1 s, the instrument's line-of-sight crosses the atmosphere at different tangent altitudes above the surface, allowing the reconstruction of the atmospheric vertical profiles.

ACS observations have been previously used to measure for the first time the vertical distribution of CO and its seasonal variations in the atmosphere of Mars (Fedorova et al., 2022; Olsen et al., 2021). Here, we use the MIR data employed by Fedorova et al., but studying the relative abundances of $^{12}C^{16}O$, $^{13}C^{16}O$ and $^{12}C^{18}O$. In particular, we use the ACS MIR measurements obtained using the secondary grating position 6, which includes fourteen diffraction orders (236-249) encompassing a spectral range between 3950-4193 cm^{-1}. We perform the retrievals in four spectral windows in diffraction orders 239 (4012-4025 cm^{-1}), 246 (4122-4142 cm^{-1}), 248 (4158-4171 cm^{-1}) and 249 (4171-4188 cm^{-1}) (see Figure 1), to retrieve the pressure, temperature and volume mixing ratios of H_2O and the aforementioned CO isotopes (see Methods). The retrieved dataset in this study comprises all ACS MIR secondary grating position 6 observations where the four presented diffraction orders were measured, which includes 242 vertical profiles mainly measured in the second halves of Martian Year (MY) 34 (L_s = 166°-349°) and MY35 (L_s = 141°-366°). This large range of observing conditions in terms of season, local time, location and dust-activity allows a better characterisation of any potential variability in the isotopic ratios, as well as to derive more reliable estimates of the measurement uncertainties.

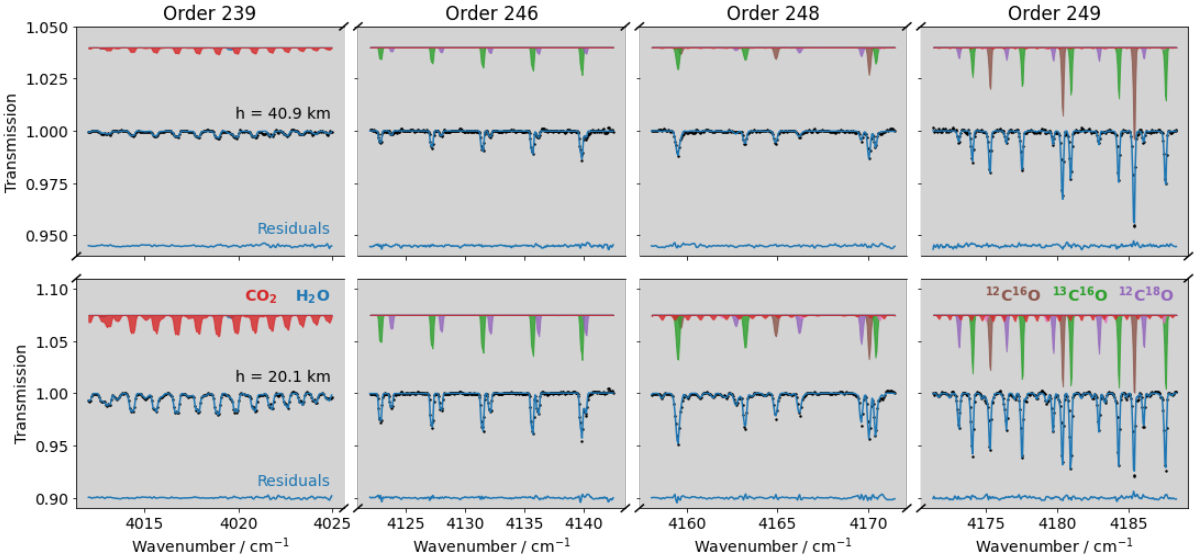

Figure 1: Example of ACS MIR spectra from secondary grating position 6 made during orbit 1896 (Latitude = 83.8°; Longitude = 170.5°; L_s = 166°; Local time = 22.5 h). The panels show the measured transmission spectra in four diffraction orders (black dots) and best fit (blue lines) at 20 (bottom) and 40 km (top). The residuals between the measurement and best fit in each diffraction order are shown in each panel, together with the contribution from each gas to each spectrum, adding a constant offset in both to improve the visibility of the figure.

Figure 2 shows a summary of all $^{13}C/^{12}C$ and $^{18}O/^{16}O$ isotopic ratios in CO measured in this dataset. We observe the $^{13}C/^{12}C$ ratio to be systematically depleted in the heavy isotopes with respect to the Earth-like standard with a weighted averaged value of $^{13}C/^{12}C$ = 0.84 ± 0.09 VPDB, where the uncertainties correspond to the standard deviation of the measurements. Comparing this value to that measured in CO_2 by the Curiosity Rover, it corresponds to a depletion of $^{13}C/^{12}C$ in CO of approximately 20%. On the other hand, the $^{18}O/^{16}O$ ratio is consistent at all altitudes with the Earth-like fractionation. The distribution of measured values in this case yields a weighted average isotopic ratio of $^{18}O/^{16}O$ = 0.98 ± 0.11 VSMOW, which compared to the isotopic ratio measured in CO_2 by the Curiosity Rover corresponds to a depletion of the O isotopic ratio in CO of 6%.

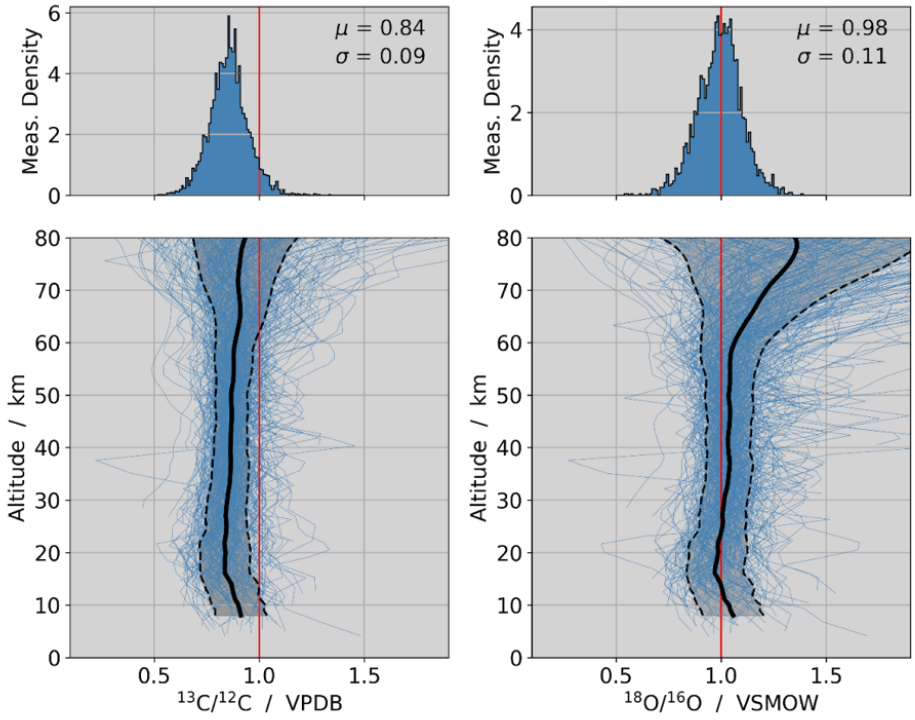

Figure 2: Vertical profiles of the C and O isotopic ratios in CO in the atmosphere of Mars. The top panels show the histogram of all measured $^{13}C/^{12}C$ and $^{18}O/^{16}O$ ratios in standard units with uncertainties lower than 0.4. The lower panels show the 242 measured vertical profiles of the isotopic ratios in this dataset (blue thin lines), as well as the weighted average (black line) and the standard deviation of the profiles (shaded areas). The red lines indicate the Earth-like standards given by Vienna Pee Dee Belemnite (VPDB) and Vienna Standard Mean Ocean Water (VSMOW).

In order to understand the physical and chemical processes that give rise to the depletion of the C and O isotopic ratios measured in CO, we constructed a 1D photochemical model to simulate the isotopic fractionation between CO and CO_2. In particular, we include isotope-specific rates for the two most important reactions relating these two species: the photolysis of CO_2 into CO + O, and the recombination of CO + OH back into CO_2. The photolysis cross-sections for $^{12}C^{16}O_2$, $^{13}C^{16}O_2$ and $^{18}O^{12}C^{16}O$ are taken from Schmidt et al. (2013), while the fractionation during the recombination of CO into CO_2 is modelled using the data from the laboratory measurements by Stevens et al. (1980) (see Methods). This photochemical model extends from the surface up to an altitude of 200 km and is set to represent martian mean dayside conditions (i.e., solar zenith angle equal to 60° and Sun-Mars distance of 1.52 AU (Krasnopolsky, 2010)). The isotopic ratios in the model are initialised assuming Earth-like fractionation at all altitudes, and the model is then run for approximately 20 years, the time by which the isotopic ratios in CO and CO_2 have converged to a steady-state solution (see Extended Data Figure 2).

Figure 3 shows the derived C isotopic abundances from the photochemical model scaled to the isotopic composition of the atmosphere of Mars measured by the Curiosity Rover, together with the measured values from the ACS observations. The C isotopic ratios in both CO and CO_2 show a similar altitudinal trend above approximately 100 km, where they continuously decrease with increasing altitude due to diffusive separation: above the homopause, where molecular diffusion dominates, species are mixed according to their own

mass-dependent scale height. As a result of this, the isotopic ratios steadily decrease with altitude, with the decrease in $^{13}C/^{12}C$ being approximately half of $^{18}O/^{16}O$ (Alday et al., 2021) (see Extended Data Figure 2). While the isotopic ratios in CO_2 below the homopause altitude are approximately constant, those in CO are depleted in the heavy isotopes due to photochemistry-induced fractionation, mainly due to the preferential photolysis of $^{12}C^{16}O_2$ over $^{13}C^{16}O_2$ and $^{18}O^{12}C^{16}O$ (see Extended Data Figures 3 and 4). In particular, the photochemical model suggests that below 30 km the C isotopic ratio in CO is approximately 24% lower than in CO_2, increasing to about 9% at 100 km. The effect of the photochemistry has a smaller impact in the O isotope ratios, with the depletion of the heavy isotopes near the surface being approximately 9%. The lower value of the $^{13}C/^{12}C$ ratio in CO than that in $^{18}O/^{16}O$ predicted by the photochemical model is consistent with the ACS measurements presented in this study.

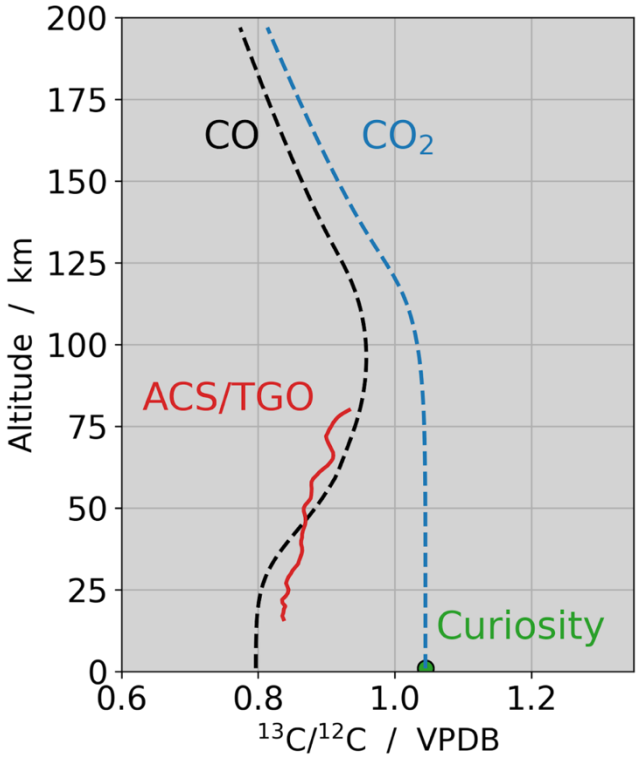

Figure 3: Photochemistry-induced fractionation of the C isotopes in the atmosphere of Mars. The ACS measurements (red) reveal a decrease of the $^{13}C/^{12}C$ isotope ratio in CO with respect to that in CO_2 measured by the Curiosity Rover at the surface (green). The predictions from the 1D photochemical model suggest that this decrease is produced by the chemistry of the martian atmosphere, which preferentially favours the transfer of ^{13}C from CO (black dashed line) to CO_2 (blue dashed line). The isotope ratio in CO in the upper atmosphere, responsible for a substantial fraction of the C escape to space, is substantially lower than that of the bulk CO_2 atmosphere, suggesting a lower escape fractionation factor than previously thought.

Both the ACS measurements and the predictions from the model suggest that the photochemistry of the atmosphere of Mars produces a depletion of the heavy C and O isotopes in CO, which represents the first direct detection of this effect in the atmosphere of Mars. Isotopic fractionation also occurs during the photolysis of other species such as H_2O, whose effect in the martian atmosphere has been extensively studied (Cheng et al., 1999; Vladimir A. Krasnopolsky, 2002). The photolysis-induced fractionation in H_2O is responsible for fractionating the D/H ratio in water, molecular hydrogen, and finally the escaping

products, giving rise to an efficient enrichment in D/H as the atmosphere escapes to space (e.g., Cangi et al. (2020); Krasnopolsky (2002)).

Since CO contributes a substantial fraction of the C escape from Mars, this new source of fractionation has to be accounted for when estimating the net escape fractionation factor. The escape of C from the atmosphere of Mars due to CO photodissociation and photoionisation is most efficient at altitudes above 150 km (Cui et al., 2019; Lo et al., 2021). At these altitudes, the isotopic composition of CO is affected by both the chemistry and diffusive separation. Our model suggests that at 200 km, the $^{13}C/^{12}C$ isotopic ratio in CO is ≈0.74 times lower than that of the bulk atmosphere, which combined with the fractionation factor due to escape by CO photodissociation ($\alpha \approx 0.6$, Hu et al. (2015)) yields a net escape fractionation factor of ≈0.44 for this reaction. This lower fractionation factor indicates that the C escape through CO photodissociation enriches the atmosphere in ^{13}C more efficiently than previously thought. In particular, considering a primordial isotopic ratio of $^{13}C/^{12}C = 0.975$ VPDB (Wright et al., 1986), and a long-term enrichment of the isotopic ratio through Rayleigh distillation, we estimate that only a loss of 12% of the atmosphere is required to have escaped to space through this mechanism to explain the enrichment of the heavy isotopes measured by the Curiosity Rover. While the total density of C on early Mars is also subject to other processes such as carbonate formation or outgassing from the surface (Hu et al., 2015), our results highlight the efficient role of this mechanism to enrich the atmosphere in the heavy isotopes, suggesting that C escape may have been less important than previously thought.

Since the atmospheric mass of ^{12}C and ^{13}C is conserved, the chemistry-induced fractionation also implies a preferential transfer of ^{13}C from CO to CO_2, which yields an enrichment in the $^{13}C/^{12}C$ ratio in CO_2. The near-surface isotopic ratio in CO_2 is found to be $\approx 3 \times 10^{-5}$ times higher than that in the initial atmosphere, which corresponds to an enrichment of $\delta^{13}C \approx 0.03$ ‰. This value is much smaller than the enrichment in the heavy isotopes observed by the Curiosity Rover ($\delta^{13}C = 46 \pm 4$ ‰, Webster et al. (2013)), which suggests that atmospheric escape remains as the preferred process contributing to the enrichment of ^{13}C in the atmosphere of Mars.

The depletion of ^{13}C in CO observed with the ACS measurements and predicted by the photochemical model is in line with the measurements of the $^{13}C/^{12}C$ ratio in Martian organics made by the Curiosity Rover (House et al., 2022). While other suggested formation mechanisms such as the photolysis of CH_4 released from the subsurface or the deposition of cosmic dust cannot be ruled out as responsible for the production of ^{13}C-depleted organics on Mars, our results confirm that the photolysis of CO_2 can produce strong depletions of the $^{13}C/^{12}C$ ratio in CO, an isotopic signature that can be transferred to formaldehyde or other organics that might accumulate on the surface of Mars.

The photochemical model also predicts a relative depletion of the $^{18}O/^{16}O$ isotopic ratio in CO with respect to CO_2, although to a lesser extent than for the C isotopes. The implications of this new source of fractionation to the long-term evolution of the O isotopes are nevertheless more complicated due to the much more complex O chemistry in the atmosphere of Mars. The dissociative recombination of O_2^+, responsible for most of the O escape from Mars (Jakosky et al., 2018), also efficiently enriches the atmosphere in ^{18}O as escape occurs (Fox & Hać, 2010). However, the overall escape fractionation factor will be subject to the $^{18}O/^{16}O$ ratio in O_2^+ and the source species of these ions (i.e., O, O^+, CO_2, CO_2^+, (Fox & Hać, 2009)), which will likely be affected by the isotope photochemistry. Based on the isotope-specific photolysis cross-sections included in this study, while the O isotopic ratios of CO_2 in the ionosphere will mostly be affected by the diffusive separation above the homopause, the isotopic composition of atomic O will be affected by the preferential photolysis of $^{12}C^{16}O_2$ over $^{18}O^{12}C^{16}O$, similar to the observed depletion of $^{18}O/^{16}O$ in CO.

However, since atomic O is produced and lost in several other chemical reactions, a comprehensive analysis of the O isotopic composition in the upper atmosphere requires a model accounting for ^{18}O in other species, which is planned but beyond the scope of the work presented here.

The results from this study highlight the important role of photochemistry in fractionating the C and O isotopic composition of the atmosphere of Mars. Future measurements of the isotopic ratios in different species may not only provide key information about the photochemical cycles in the atmosphere of Mars, but also provide accurate estimations of the fractionation between the lower and upper atmospheres, which has important implications to our understanding of the long-term evolution of Mars' climate.

2. Methods

2.1 Retrieval scheme

The inversion of the spectra is performed using the NEMESIS algorithm (Irwin et al., 2008), applying the same two-step methodology as in Alday et al. (2021). First, the pressure and temperature profiles are determined using the CO_2 absorption features in diffraction order 239 (see Figure 1). Secondly, the pressure and temperature are fixed, and the abundances of the trace gases (i.e., H_2O, $^{12}C^{16}O$, $^{13}C^{16}O$ and $^{12}C^{18}O$) are retrieved using all diffraction orders. All gaseous absorption in this study is modelled using pre-computed line-by-line look-up tables generated using the spectroscopic parameters from the 2020 edition of the HITRAN database (Gordon et al., 2022). Apart from the retrieval of the atmospheric parameters, the instrument line shape (ILS) is also fitted in each occultation using a double Gaussian parameterisation (Alday et al., 2019).

The pressure and temperature profiles are retrieved under the assumption of an atmosphere in hydrostatic equilibrium and a known CO_2 volume mixing ratio. This approach has been widely used in the past to determine the thermal structure of the atmosphere of Mars from solar occultation observations (Forget et al., 2009; Montmessin et al., 2006; Quémerais et al., 2006). The retrieval scheme from the NEMESIS algorithm works using the optimal estimation framework, which aims to find an optimal solution that is consistent with the observed spectra subject to a minimal departure from the *a priori*. Given that the absorption features of CO_2 measured in ACS MIR secondary grating position 6 typically disappear at lower tangent altitudes than the CO ones, we use temperature profiles from simultaneous observations by ACS NIR (Fedorova et al., 2022) as the *a priori* in our retrievals, which ensures an accurate description of the temperature field at all altitudes. The use of accurate measurements of temperature is crucial to derive precise measurements of the CO isotopic ratios, which are highly sensitive to this parameter (see Supplementary Material).

Once the pressure and temperature profiles are determined, these are fixed, and the gaseous abundances of the CO isotopes and H_2O are retrieved. In this case, the *a priori* information is taken from the OpenMARS reanalysis dataset (Holmes et al., 2020), which assimilates the temperature profiles and dust opacities measured by the Mars Climate Sounder onboard the Mars Reconnaissance Orbiter into the General Circulation Model. The *a priori* isotopic composition is assumed to follow that of Earth-like conditions given by the Vienna Pee Dee Belemnite ($^{13}C/^{12}C$ = 1 VPDB = 0.0112372) and the Vienna Standard Mean Ocean Water ($^{18}O/^{16}O$ = 1 VSMOW = 0.0020052). Given that the sensitivity of the retrieval to the CO isotopes can be different at different altitudes (i.e., the $^{12}C^{18}O$ absorption lines typically disappear at lower tangent heights than the $^{12}C^{16}O$), the influence of the *a priori* guess in the retrieval of the isotopologues might also be different. Therefore, in order to ensure no biases from the *a priori* are introduced into the derivations of the isotopic ratios, the retrievals are run twice, the second time using the retrieved $^{12}C^{16}O$ abundances from the previous iteration as the *a priori* and scaling the abundances of the minor isotopes with the same Earth-like isotopic ratios.

In each acquisition made by ACS MIR, the observed diffraction orders encompass about 20 detector rows, which correspond to the instantaneous field-of-view of the instrument, with each row sampling slightly different tangent heights ($\Delta z \approx 150$ m per row). In addition, the ILS varies from row to row, which can introduce systematic uncertainties in the retrievals. In order to increase the confidence of the retrievals and better understand the uncertainties arising from the ILS fitting, we apply the retrieval scheme to seven detector rows. The retrieved profiles from each row are then combined using a weighted average. The uncertainties are calculated considering both the error of the mean, and the standard deviation of the profiles (Alday et al., 2021). We consider this method for calculating the

uncertainties to provide a more accurate representation of the true uncertainty of the retrieval in which not only the random uncertainties, but also the systematic ones are captured.

A detailed validation of the retrievals presented in this study is provided in the Supplementary Material.

2.2 Photochemical model

The 1D photochemical model aims to solve the continuity equation given by

$$\frac{\partial n_i}{\partial t} = P_i - L_i - \frac{\partial \phi_i}{\partial z},$$

where n_i is the number density of a given species, P_i and L_i represent the production and loss of density due to the photochemical reactions, and the last term represents the diffusion between layers, where ϕ is the flux. The flux is calculated considering both Eddy and molecular diffusion and is given by

$$\phi_i = -(K + D_i)\frac{\partial n_i}{\partial z} - n_i\left[K\left(\frac{1}{H_0} + \frac{1}{T}\frac{\partial T}{\partial z}\right) + D_i\left(\frac{1}{H_i} + \frac{(1+\alpha)}{T}\frac{\partial T}{\partial z}\right)\right],$$

where K and D_i are the Eddy and molecular diffusion coefficients, H_0 is the mean scale height, H_i is the gas-dependent scale height, α is the thermal diffusion coefficient, and T is the temperature.

The diffusion term is calculated by finite differences, using an approach similar to Krasnopolsky (1993), which yields

$$\frac{\partial \phi_{i,j}}{\partial z} \sim -\left(k_j + d_{i,j}\right)\cdot n_{i,j+1} + \left(kl_j + dl_{i,j} + k_{j-1} + d_{i,j-1}\right)\cdot n_{i,j} - \left(kl_{j-1} + dl_{i,j-1}\right)\cdot n_{i,j-1}$$

where the subscripts i and j represent the gas and layer, respectively. The coefficients in the finite differences approximation are given by

$$k_j = \frac{K_{j+1/2}}{\Delta z^2},$$

$$d_{i,j} = \frac{D_{i,j+1/2}}{\Delta z^2},$$

$$kl_j = k_j \cdot \left(1 - \frac{\Delta z}{H_{0_{j+\frac{1}{2}}}} - \frac{T_{j+1} - T_j}{T_{j+\frac{1}{2}}}\right),$$

$$dl_{i,j} = d_{i,j} \cdot \left(1 - \frac{\Delta z}{H_{i,j+\frac{1}{2}}} - (1+\alpha)\cdot\frac{T_{j+1} - T_j}{T_{j+\frac{1}{2}}}\right),$$

where Δz is the altitude of each layer.

The production and loss terms are calculated using the latest version of the photochemical scheme from the Mars Planetary Climate Model (PCM) , which has been extensively used to

model the photochemical cycles in the atmosphere of Mars (Cariolle et al., 2017; Lefèvre et al., 2021; Lefèvre et al., 2004). This scheme includes 14 chemical species and 39 chemical reactions to model the photochemistry of H, C and O in the atmosphere of Mars. Here, we introduce four new species ($^{13}C^{16}O_2$, $^{13}C^{16}O$, $^{18}O^{12}C^{16}O$ and $^{12}C^{18}O$) and ten chemical reactions to model the isotopic fractionation between CO_2 and CO. The reaction rates are calculated assuming mean dayside conditions with a constant solar zenith angle of 60° and a constant Sun-Mars distance of 1.52 AU.

The reactions included to model the ^{13}C chemistry are:

$^{13}CO_2 + hv \rightarrow {}^{13}CO + O \quad (\lambda > 167\ nm)$
$^{13}CO_2 + hv \rightarrow {}^{13}CO + O(^1D) \quad (\lambda < 167\ nm)$

$^{13}CO + O + M \rightarrow {}^{13}CO_2 + M$

$^{13}CO + OH \rightarrow {}^{13}CO_2 + H$

The reactions included to model the O fractionation between CO_2 and CO are:

$^{18}OC^{16}O + hv \rightarrow C^{18}O + {}^{16}O \quad (\lambda > 167\ nm)$
$^{18}OC^{16}O + hv \rightarrow C^{16}O + {}^{16}O \quad (\lambda > 167\ nm)$

$^{18}OC^{16}O + hv \rightarrow C^{18}O + {}^{16}O(^1D) \quad (\lambda < 167\ nm)$
$^{18}OC^{16}O + hv \rightarrow C^{16}O + {}^{16}O(^1D) \quad (\lambda < 167\ nm)$

$C^{18}O + {}^{16}O + M \rightarrow {}^{18}OC^{16}O + M$

$C^{18}O + {}^{16}OH \rightarrow {}^{18}OC^{16}O + H$

It must be noted that in the version for the ^{18}O chemistry the total mass is not conserved, as we do not include ^{18}O or $^{18}O(^1D)$ in the chemistry scheme. These species, together with the definition of the ^{18}O isotopologues in other O-bearing species are necessary to model the complete chemistry of ^{18}O in the atmosphere of Mars. Here, we just aim to model the relative fractionation of the $^{18}O/^{16}O$ isotopic ratio between CO_2 and CO, which is not expected to be affected by this simplification, since CO molecules are solely produced by the photolysis of CO_2, which is included in the scheme.

The continuity equation is solved using a second-order Rosenbrock algorithm (Hobbs et al., 2019; Verwer et al., 1999). The density at the next time step is calculated following

$$n^{t+1} = n^t + 1.5\Delta t \cdot g_1 + 0.5\Delta t \cdot g_2,$$
$$(I - \gamma \Delta t J) g_1 = f(n^t),$$
$$(I - \gamma \Delta t J) g_2 = f(n^t - \Delta t g_1) - 2 g_1,$$

Where $\gamma = 1 + 1/\sqrt{2}$, Δt is the time step, $f(n)$ is the right-hand side of the differential equation (i.e., the chemistry and transport terms evaluated at the density n) and J is the Jacobian matrix of the combined chemistry-transport system. Since the densities of a given species at a given layer are only influenced by the densities of the other gases in the same layer (i.e., chemistry) and the densities of the same gas in the adjacent layers (i.e., diffusion), the Jacobian matrix takes the form of a block tridiagonal matrix, which is efficiently inverted using the Thomas algorithm (Hu et al., 2012).

The choice of the time step is made based on the maximum local error, which is estimated by the difference between the first-order and second-order solutions, following

$$\varepsilon = n^{t+1} - n_1^{t+1} = (n^t + 1.5\Delta t \cdot g_1 + 0.5\Delta t \cdot g_2) - (n^t + \Delta t \cdot g_1).$$

The timestep is self-adjusted by $\Delta t^{t+1} \sim \Delta t^t / \sqrt{\varepsilon_{max}}$, which ensures that the convergence of the system to a steady-state solution will capture the orders-of-magnitude difference in the chemical and diffusion timescales while optimising the computational time.

The 1D photochemical model requires several inputs to represent the composition and mixing of the atmosphere of Mars. The initial temperature and density profiles are derived using an average of vertical profiles generated from the Mars Climate Database (Forget et al., 1999) at different times and locations. In particular, we generate vertical profiles of temperature, number density and volume mixing ratios from 0 to 200 km in a grid of latitudes, local times and solar longitude L_S. The latitudes expand from -80° to 80° with a step of 20°. The local time expands from 0 to 24 hours with a two-hour step. The L_S expands the whole year, with a step of 10°. The calculated profiles are then averaged using the atmospheric density as a weight (see Extended Data Figure 1). The abundances of CO_2 and CO from the Mars Climate Database are then divided into the different isotopologues by assuming a given isotopic ratio, and using

$$[^{12}C^{16}O_2] = [CO_2] / (1 + R)$$
$$[^{13}C^{16}O_2] = [^{12}C^{16}O_2] \times R$$

where the bracketed quantities represent the abundances of the different species, and R is the assumed Earth-like isotopic ratio (i.e., $^{13}C/^{12}C$ = 1 VPDB and $^{18}O/^{16}O$ = 1 VSMOW).

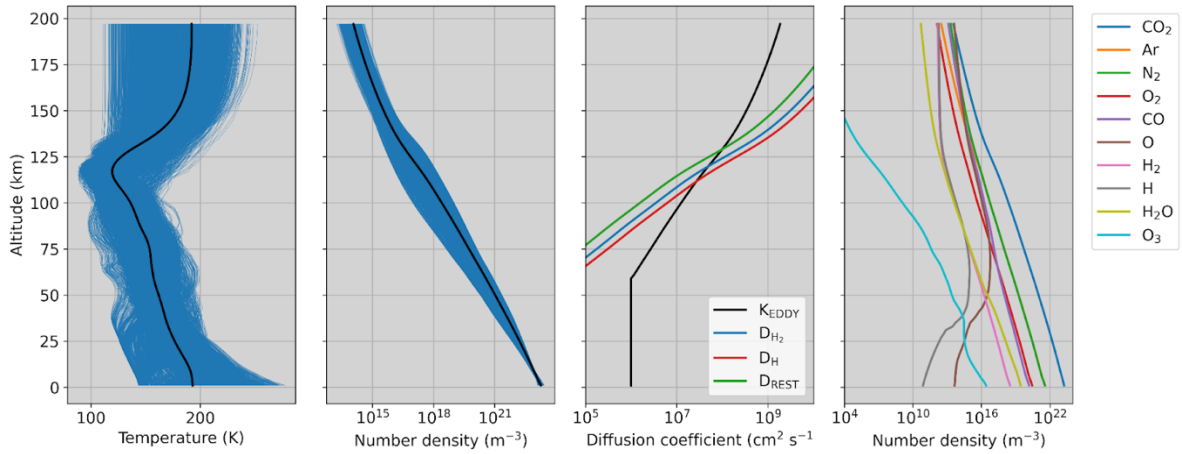

Extended Data Figure 1: Overview of the main inputs for the photochemical model. The initial profiles for the temperature, total number density and partial number density are calculated by averaging profiles from the Mars Climate Database throughout different seasons, locations and local time. The Eddy and molecular diffusion coefficients are calculated from Krasnopolsky (1993) and using the coefficients from Hunten (1973), respectively.

The diffusion coefficients assumed in our Mars 1D photochemical model are the same as those used by Chaffin et al. (2017) and Cangi et al. (2020), which were taken from other previous studies (e.g., Hunten (1973); Krasnopolsky (1993)). In particular, the Eddy diffusion coefficient is given by

$K(z < 60\ km) = 10^6$ cm^2 s^{-1},
$K(z < 60\ km) = 2 \cdot 10^{13} \cdot n(z)^{-1/2}$ cm^2 s^{-1},

as shown in Extended Data Figure 1. The molecular diffusion coefficient is given by

$$D(z) = \frac{AT(z)^s}{n(z)}.$$

The coefficients *A* and *s* for H_2 and H are given by Hunten, (1973), which are equal to A_H = *8.4 x 10^{17}*, s_H = *0.597*, A_{H2} = *2.23 × 10^{17}*, s_{H2} = *0.75.* For the rest of the species, we adopt *A* = *10^{17}* and *s* = *0.75* (see Extended Data Figure 1).

The boundary conditions are similar to those used in Chaffin et al. (2017). We consider the top boundary conditions to be a zero flux for all species but for H_2, H and O. For H_2 and H, we fix their escaping velocities to be v_{H2} = *3.4 x 10^1* cm s^{-1} and v_H = *3.1 x 10^3* cm s^{-1}, while for O we fix the escaping flux to be ϕ_O = *1.2 x 10^8* cm^{-2} s^{-1}. For the lower boundary conditions, we set a zero flux for all species, but for H_2O, whose density is assumed to be fixed below 50 km.

Using these inputs and the presented model setup, we run a simulation for 20 years, the time by which the O and C isotopic ratios in both CO and CO_2 have converged to a steady-state solution, as it is shown in Extended Data Figure 2.

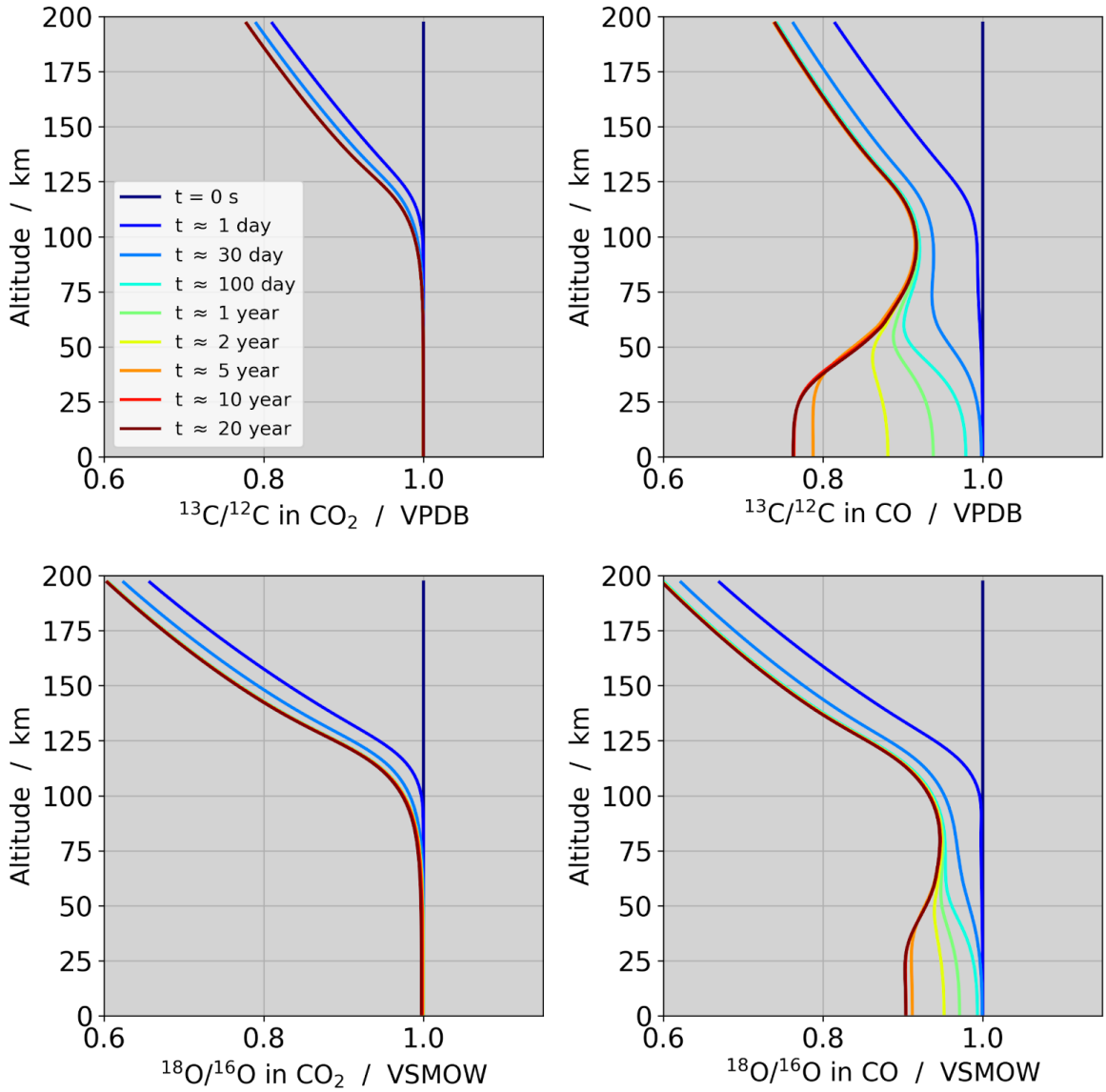

Extended Data Figure 2: Evolution of the isotopic ratios in the 1D photochemical model. The four panels show the carbon (top) and oxygen (bottom) isotopic ratios in CO_2 (left) and CO (right) as a function of time as the simulation from the photochemical model progresses. The isotopic ratios in CO_2 converge rapidly, as they are mostly affected by diffusive separation, which produces a decrease of the isotopic ratios above the homopause according to their own mass-dependent scale heights. The isotopic ratios in CO are affected by both diffusive separation and by the photochemistry-induced fractionation. The photochemistry of the atmosphere produces a depletion in the $^{13}C/^{12}C$ and $^{18}O/^{16}O$ ratios, whose effect is stronger for the former of the two, consistent with the ACS observations.

2.3 Fractionation during the photolysis of CO_2

The photolysis cross sections of CO_2 used in the chemistry scheme of the LMD Mars PCM are a composite of different laboratory measurements in different spectral ranges (Huestis & Berkowitz, 2010; Lewis & Carver, 1983; Parkinson et al., 2003; Stark et al., 2007; Yoshino et al., 1996) and tabulated at temperatures of 195, 295 and 370 K (Lefèvre et al., 2021). In order to model the fractionation factor of this reaction, we use the photolysis cross sections calculated by Schmidt et al. (2013) for $^{12}C^{16}O_2$, $^{13}C^{16}O_2$ and $^{18}O^{12}C^{16}O$ between 150-210 nm, which are combined with the Mars PCM reference for <150nm at 195, 295 and 370 K.

Extended Data Figure 3 shows how the calculated cross sections for $^{12}C^{16}O_2$ compare with those tabulated in the chemistry scheme, together with a comparison between the cross sections calculated for the different isotopologues. These results suggest that the photolysis cross sections of $^{12}C^{16}O_2$ are larger than those of the minor isotopes (i.e., $^{13}C^{16}O_2$ and $^{18}O^{12}C^{16}O$) by a factor of 1.0-1.5 and 1.0-1.3, respectively. The ratio between the cross sections of $^{12}C^{16}O_2$ and those of the minor isotopes also depends on the temperature, with that at 195 K being on average 5% larger than that at 295 K.

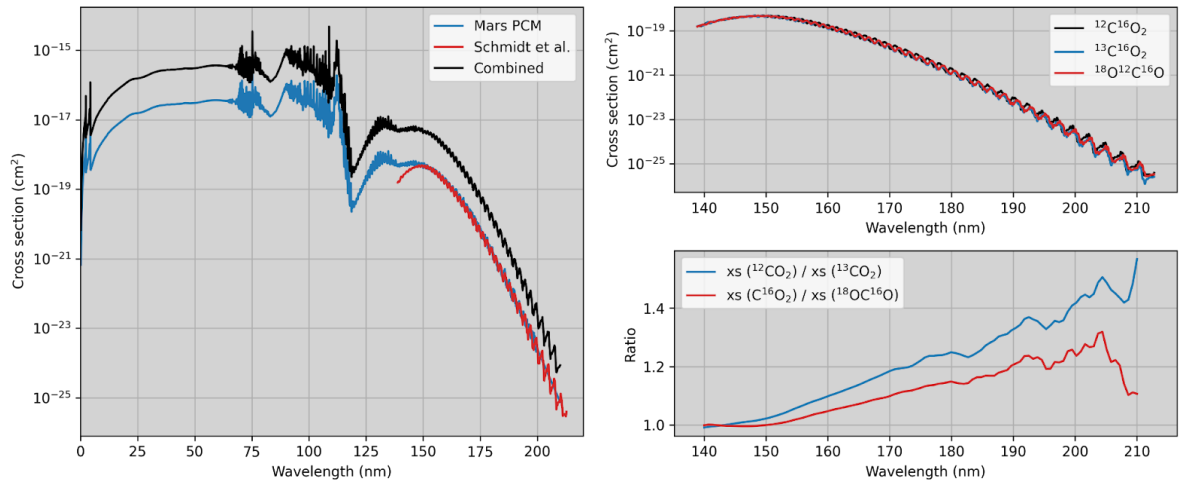

Extended Data Figure 3: Summary of the photolysis cross sections used in this study. The left plot shows a comparison between the cross sections tabulated in the Mars PCM (blue line) and those calculated by Schmidt et al. (2013) (red line) at 295 K. In addition, the combined cross sections used in this study are shown with a x10 offset. The top right plot shows the cross sections calculated by Schmidt et al. (2013) for the different isotopologues. The bottom right plot shows the ratio between the cross sections of the major and minor isotopes, convolved with a Gaussian function with a FWHM of 2.5nm to smooth out high frequency variations.

It is important to note that the cross sections for the minor isotopes are only available for a limited spectral range (>150 nm), and these are lower than the cross sections elsewhere (<150 nm), where we assume that they are equal for all isotopes. In order to evaluate where the cross sections >150 nm are most effective in the photolysis of CO_2 molecules in the atmosphere of Mars, we calculate the photolysis *J*-values as a function of altitude (see Extended Data Figure 4). These results show that the *J*-values are approximately constant above ≈100 km, where the atmosphere is optically thin. Below this altitude, the atmosphere becomes optically thick for wavelengths lower than 150 nm, and the *J*-values decrease with decreasing altitude as the atmosphere also becomes optically thick for wavelengths >150 nm. Therefore, while the cross sections <150 nm are important above 100 km, their effect becomes negligible below 100 km, the region where the ACS observations can measure the isotopic fractionation between CO_2 and CO.

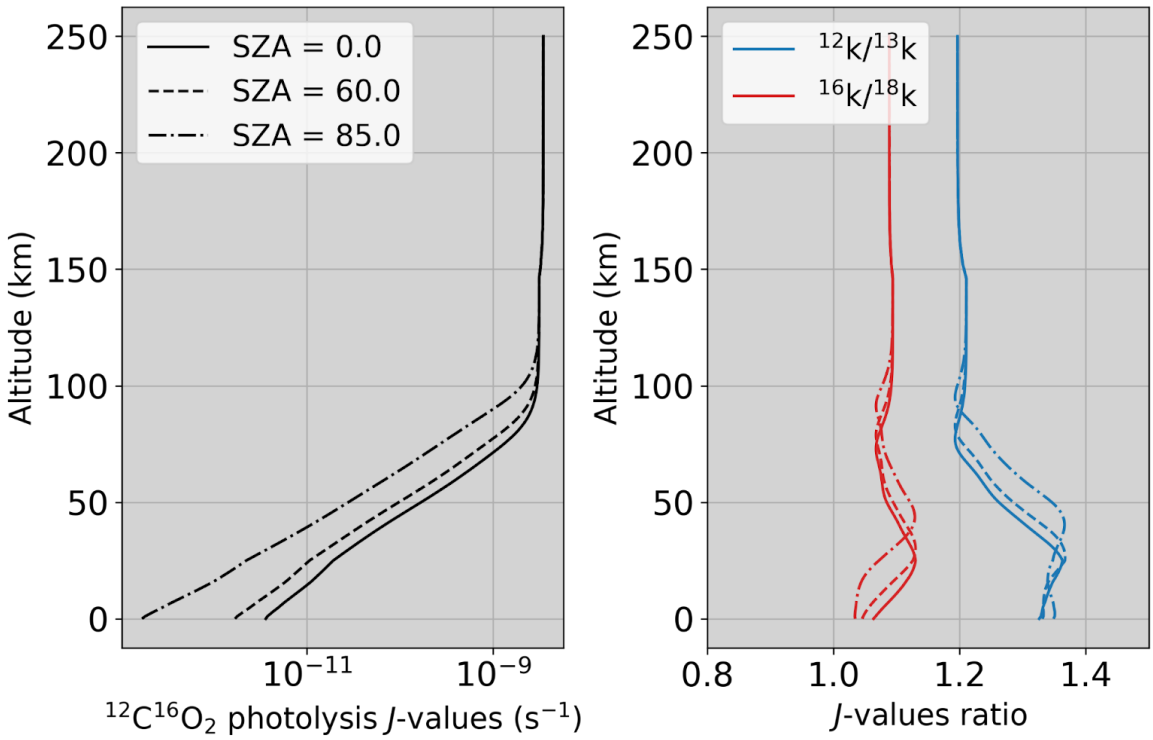

Extended Data Figure 4: Photolysis J-values of $^{12}C^{16}O_2$ and the isotope effect. The left-hand panel shows the calculated photolysis J-values of the $^{12}C^{16}O_2$ at three different solar zenith angles. The right-hand panel shows the ratio between the photolysis rates of $^{12}C^{16}O_2$ over those of $^{13}C^{16}O_2$ and $^{18}O^{12}C^{16}O$.

The right-hand panel of Extended Data Figure 4 shows the ratio between the photolysis rates of $^{12}C^{16}O_2$ over those of $^{13}C^{16}O_2$ and $^{18}O^{12}C^{16}O$, which is higher than one at all altitudes. These results suggest that the photolysis of $^{12}C^{16}O_2$ is faster than that of the minor isotopes, meaning that $^{12}C^{16}O$ will be more efficiently produced than $^{13}C^{16}O$ and $^{12}C^{18}O$. The net effect of this process is to produce a depletion of the $^{13}C/^{12}C$ and $^{18}O/^{16}O$ ratios in CO with respect to those in CO_2, and the magnitude of this effect is larger for the C isotopes than the O ones.

2.4 Fractionation during the recombination of CO + OH

The recombination of CO with the hydroxyl radical OH is an important reaction in the chemistry of the atmosphere of Mars, which is responsible for the stability of CO_2 (McElroy & Donahue, 1972; Parkinson & Hunten, 1972). In order to model the isotopic fractionation of the C and O isotopes in this reaction, we use the data derived from laboratory measurements by Stevens et al. (1980). These measurements determined the kinetic isotope effect at a range of pressures from 0.2 to 1.35 atm (see Extended Data Figure 5). In order to extrapolate the measurements to the low pressure of the martian atmosphere, we fit this dependence using a second-order polynomial function. The fitted polynomial functions for the C and O isotopes are respectively

$$k^{13}/_{k^{12}} = 1.00638 - 1.69300 \times 10^{-7} \cdot p + 4.69677 \times 10^{-13} \cdot p^2,$$

$$k^{18}/_{k^{12}} = 1.01195 - 4.44340 \times 10^{-7} \cdot p + 1.93835 \times 10^{-13} \cdot p^2,$$

where the ratios $^{13}k/^{12}k$ and $^{18}k/^{16}k$ represent the ratio between the reaction rates of the minor isotopes (i.e., ^{13}CO and $C^{18}O$) with respect to that of the major one (i.e., $^{12}C^{16}O$) and *p* is the pressure in Pascals.

At the low pressures of the martian atmosphere, this reaction is faster for the minor isotopes, which yields a preferential transfer of ^{13}C and ^{18}O over ^{12}C and ^{16}O from CO to CO_2. Therefore, the net effect of this reaction is to produce a depletion of the $^{13}C/^{12}C$ and $^{18}O/^{16}O$ isotopic ratios in CO with respect to CO_2. However, given the small magnitude of this fractionation factor with respect to that produced by the photolysis of CO_2, this process is expected to have a much minor effect in the overall fractionation between CO_2 and CO.

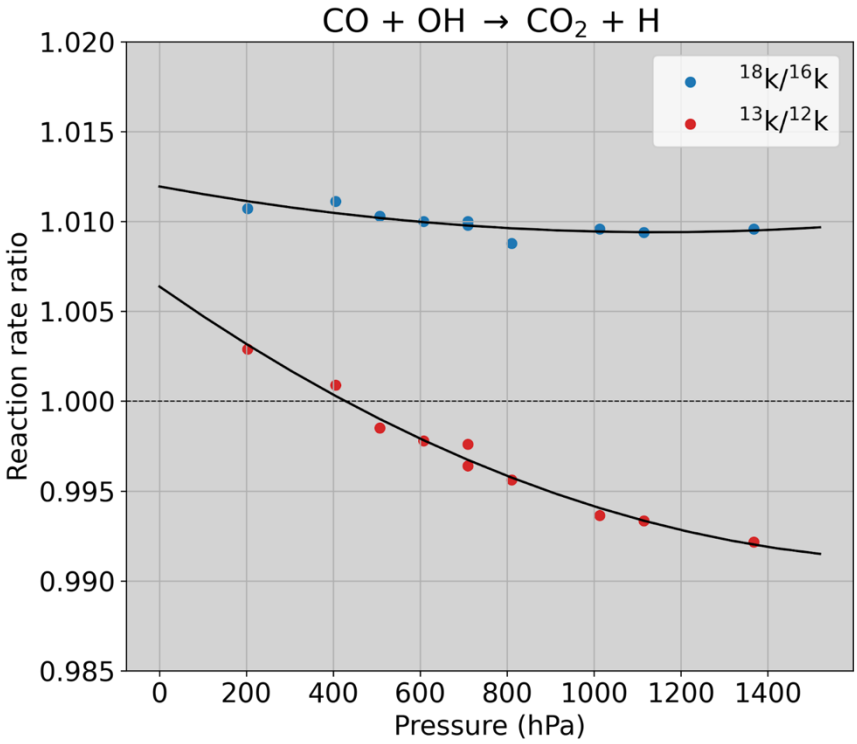

Extended Data Figure 5: Isotopic fractionation during the recombination of CO and OH into CO_2 and H. The blue and red dots represent the ratio between the reaction rates of $C^{18}O/C^{16}O$ and $^{13}CO/^{12}CO$, measured by Stevens et al. (1988). The black lines are a second-order polynomial fit used to capture the pressure dependence of this fractionation effect.

3. References

Alday, J., Wilson, C. F., Irwin, P. G. J., Olsen, K. S., Baggio, L., Montmessin, F., et al. (2019). Oxygen isotopic ratios in Martian water vapour observed by ACS MIR on board the ExoMars Trace Gas Orbiter. *Astronomy & Astrophysics*, *630*, A91. https://doi.org/10.1051/0004-6361/201936234

Alday, Juan, Wilson, C. F., Irwin, P. G. J., Trokhimovskiy, A., Montmessin, F., Fedorova, A. A., et al. (2021). Isotopic Composition of CO_2 in the Atmosphere of Mars: Fractionation by Diffusive Separation Observed by the ExoMars Trace Gas Orbiter. *Journal of Geophysical Research: Planets*, *126*(12). https://doi.org/10.1029/2021JE006992

Alday, Juan, Trokhimovskiy, A., Irwin, P. G. J., Wilson, C. F., Montmessin, F., Lefévre, F., et al. (2021). Isotopic fractionation of water and its photolytic products in the atmosphere of Mars. *Nature Astronomy*. https://doi.org/10.1038/s41550-021-01389-x

Baker, V. R. (2001). Water and the martian landscape. *Nature*, *412*(6843), 228–236. https://doi.org/10.1038/35084172

Cangi, E. M., Chaffn, M. S., & Deighan, J. (2020). Higher Martian atmospheric temperatures at all altitudes increase the D/H fractionation factor and water loss. *Journal of Geophysical Research: Planets*, *125*(12), e2020JE006626. https://doi.org/10.1029/2020JE006626

Cariolle, D., Moinat, P., Teyssèdre, H., Giraud, L., Josse, B., & Lefèvre, F. (2017). ASIS v1.0: an adaptive solver for the simulation of atmospheric chemistry. *Geoscientific Model Development*, *10*(4), 1467–1485. https://doi.org/10.5194/gmd-10-1467-2017

Carr, M. H., & Clow, G. D. (1981). Martian channels and valleys: Their characteristics, distribution, and age. *Icarus*, *48*(1), 91–117. https://doi.org/10.1016/0019-1035(81)90156-1

Chaffin, M. S., Deighan, J., Schneider, N. M., & Stewart, A. I. F. (2017). Elevated atmospheric escape of atomic hydrogen from Mars induced by high-altitude water. *Nature Geoscience*, *10*(3), 174–178. https://doi.org/10.1038/ngeo2887

Cheng, B.-M., Chew, E. P., Liu, C.-P., Bahou, M., Lee, Y.-P., Yung, Y. L., & Gerstell, M. F. (1999). Photo-induced fractionation of water isotopomers in the Martian atmosphere. *Geophysical Research Letters*, *26*(24), 3657–3660. https://doi.org/10.1029/1999GL008367

Cui, J., Wu, X.-S., Gu, H., Jiang, F.-Y., & Wei, Y. (2019). Photochemical escape of atomic C and N on Mars: clues from a multi-instrument MAVEN dataset. *Astronomy & Astrophysics*, *621*, A23. https://doi.org/10.1051/0004-6361/201833749

Fedorova, A., Trokhimovskiy, A., Lefèvre, F., Olsen, K. S., Korablev, O., Montmessin, F., et al. (2022). Climatology of the CO Vertical Distribution on Mars Based on ACS TGO Measurements. *Journal of Geophysical Research: Planets*, *127*(9). https://doi.org/10.1029/2022JE007195

Forget, F., Hourdin, F., Fournier, R., Hourdin, C., Talagrand, O., Collins, M., et al. (1999). Improved general circulation models of the Martian atmosphere from the surface to above 80 km. *Journal of Geophysical Research: Planets*, *104*(E10), 24155–24175. https://doi.org/10.1029/1999JE001025

Forget, F., Montmessin, F., Bertaux, J.-L., González-Galindo, F., Lebonnois, S., Quémerais, E., et al. (2009). Density and temperatures of the upper Martian atmosphere measured by stellar occultations with Mars Express SPICAM. *Journal of Geophysical Research*, *114*(E1), E01004. https://doi.org/10.1029/2008JE003086

Fox, J. L., & Hać, A. (1999). Velocity distributions of C atoms in CO^+ dissociative recombination: Implications for photochemical escape of C from Mars. *Journal of Geophysical Research: Space Physics*, *104*(A11), 24729–24737. https://doi.org/10.1029/1999JA900330

Fox, Jane L., & Hać, A. (2010). Isotope fractionation in the photochemical escape of O from Mars. *Icarus*, *208*(1), 176–191. https://doi.org/10.1016/j.icarus.2010.01.019

Fox, Jane L., & Hać, A. B. (2009). Photochemical escape of oxygen from Mars: A comparison of the exobase approximation to a Monte Carlo method. *Icarus*, *204*(2), 527–544. https://doi.org/10.1016/j.icarus.2009.07.005

Gordon, I. E., Rothman, L. S., Hargreaves, R. J., Hashemi, R., Karlovets, E. V., Skinner, F. M., et al. (2022). The HITRAN2020 molecular spectroscopic database. *Journal of Quantitative Spectroscopy and Radiative Transfer*, *277*, 107949. https://doi.org/10.1016/j.jqsrt.2021.107949

Gröller, H., Lichtenegger, H., Lammer, H., & Shematovich, V. I. (2014). Hot oxygen and carbon escape from the martian atmosphere. *Planetary and Space Science*, *98*, 93–105. https://doi.org/10.1016/j.pss.2014.01.007

Head, J. W., Hiesinger, H., Ivanov, M. A., Kreslavsky, M. A., Pratt, S., & Thomson, B. J. (1999). Possible Ancient Oceans on Mars: Evidence from Mars Orbiter Laser Altimeter Data. *Science*, *286*(5447), 2134–2137. https://doi.org/10.1126/science.286.5447.2134

Hobbs, R., Shorttle, O., Madhusudhan, N., & Rimmer, P. (2019). A chemical kinetics code for modelling exoplanetary atmospheres. *Monthly Notices of the Royal Astronomical Society*, *487*(2), 2242–2261. https://doi.org/10.1093/mnras/stz1333

Holmes, J. A., Lewis, S. R., & Patel, M. R. (2020). OpenMARS: A global record of martian weather from 1999 to 2015. *Planetary and Space Science*, *188*, 104962. https://doi.org/10.1016/j.pss.2020.104962

House, C. H., Wong, G. M., Webster, C. R., Flesch, G. J., Franz, H. B., Stern, J. C., et al. (2022). Depleted carbon isotope compositions observed at Gale crater, Mars. *Proceedings of the National Academy of Sciences*, *119*(4), e2115651119. https://doi.org/10.1073/pnas.2115651119

Hu, R., & Thomas, T. B. (2022). A nitrogen-rich atmosphere on ancient Mars consistent with isotopic evolution models. *Nature Geoscience*, *15*(2), 106–111. https://doi.org/10.1038/s41561-021-00886-y

Hu, R., Seager, S., & Bains, W. (2012). PHOTOCHEMISTRY IN TERRESTRIAL EXOPLANET ATMOSPHERES. I. PHOTOCHEMISTRY MODEL AND BENCHMARK CASES. *The Astrophysical Journal*, *761*(2), 166. https://doi.org/10.1088/0004-637X/761/2/166

Hu, R., Kass, D. M., Ehlmann, B. L., & Yung, Y. L. (2015). Tracing the fate of carbon and the atmospheric evolution of Mars. *Nature Communications*, *6*(1), 10003. https://doi.org/10.1038/ncomms10003

Huestis, D. L., & Berkowitz, J. (2010). Critical Evaluation of the Photoabsorption Cross Section of CO2 from 0.125 to 201.6 nm at Room Temperature, *42*, 48.13. Presented at the AAS/Division for Planetary Sciences Meeting Abstracts #42.

Hunten, D. M. (1973). The Escape of Light Gases from Planetary Atmospheres. *Journal of the Atmospheric Sciences*, *30*(8), 1481–1494. https://doi.org/10.1175/1520-0469(1973)030<1481:TEOLGF>2.0.CO;2

Irwin, P. G. J., Teanby, N. A., de Kok, R., Fletcher, L. N., Howett, C. J. A., Tsang, C. C. C., et al. (2008). The NEMESIS planetary atmosphere radiative transfer and retrieval tool. *Journal of Quantitative Spectroscopy and Radiative Transfer*, *109*(6), 1136–1150. https://doi.org/10.1016/j.jqsrt.2007.11.006

Jakosky, B. M., Slipski, M., Benna, M., Mahaffy, P., Elrod, M., Yelle, R., et al. (2017). Mars' atmospheric history derived from upper-atmosphere measurements of $^{38}Ar/^{36}Ar$. *Science*, *355*(6332), 1408–1410. https://doi.org/10.1126/science.aai7721

Jakosky, B.M., Brain, D., Chaffin, M., Curry, S., Deighan, J., Grebowsky, J., et al. (2018). Loss of the Martian atmosphere to space: Present-day loss rates determined from MAVEN observations and integrated loss through time. *Icarus*, *315*, 146–157. https://doi.org/10.1016/j.icarus.2018.05.030

Jakosky, Bruce M. (2019). The CO2 inventory on Mars. *Planetary and Space Science*, *175*, 52–59. https://doi.org/10.1016/j.pss.2019.06.002

Korablev, O., Montmessin, F., Trokhimovskiy, A., Fedorova, A. A., Shakun, A. V., Grigoriev, A. V., et al. (2018). The Atmospheric Chemistry Suite (ACS) of Three Spectrometers for the ExoMars 2016 Trace Gas Orbiter. *Space Science Reviews*, *214*(1), 7. https://doi.org/10.1007/s11214-017-0437-6

Krasnopolsky, V.A. (1993). Photochemistry of the Martian Atmosphere (Mean Conditions). *Icarus*, *101*(2), 313–332. https://doi.org/10.1006/icar.1993.1027

Krasnopolsky, Vladimir A. (2002). Mars' upper atmosphere and ionosphere at low, medium, and high solar activities: Implications for evolution of water. *Journal of Geophysical Research: Planets*, *107*(E12), 11–1. https://doi.org/10.1029/2001JE001809

Krasnopolsky, Vladimir A. (2010). Solar activity variations of thermospheric temperatures on Mars and a problem of CO in the lower atmosphere. *Icarus*, *207*(2), 638–647. https://doi.org/10.1016/j.icarus.2009.12.036

Krasnopolsky, Vladimir A., Mumma, M. J., & Gladstone, G. R. (1998). Detection of Atomic Deuterium in the Upper Atmosphere of Mars. *Science*, *280*(5369), 1576–1580. https://doi.org/10.1126/science.280.5369.1576

Lefèvre, F., Trokhimovskiy, A., Fedorova, A., Baggio, L., Lacombe, G., Määttänen, A., et al. (2021). Relationship Between the Ozone and Water Vapor Columns on Mars as Observed by SPICAM and Calculated by a Global Climate Model. *Journal of Geophysical Research: Planets*, *126*(4). https://doi.org/10.1029/2021JE006838

Lefèvre, Franck, Lebonnois, S., Montmessin, F., & Forget, F. (2004). Three-dimensional modeling of ozone on Mars. *Journal of Geophysical Research: Planets*, *109*(E7). https://doi.org/10.1029/2004JE002268

Lewis, B. R., & Carver, J. H. (1983). Temperature dependence of the carbon dioxide photoabsorption cross section between 1200 and 1970 Å. *Journal of Quantitative Spectroscopy and Radiative Transfer*, *30*(4), 297–309. https://doi.org/10.1016/0022-4073(83)90027-4

Lo, D. Y., Yelle, R. V., Lillis, R. J., & Deighan, J. I. (2021). Carbon photochemical escape rates from the modern Mars atmosphere. *Icarus*, *360*, 114371. https://doi.org/10.1016/j.icarus.2021.114371

Mahaffy, P. R., Webster, C. R., Atreya, S. K., Franz, H., Wong, M., Conrad, P. G., et al. (2013). Abundance and Isotopic Composition of Gases in the Martian Atmosphere from the Curiosity Rover. *Science*, *341*(6143), 263–266. https://doi.org/10.1126/science.1237966

McElroy, M. B. (1972). Mars: An Evolving Atmosphere. *Science*, *175*(4020), 443–445. https://doi.org/10.1126/science.175.4020.443

McElroy, M. B., & Donahue, T. M. (1972). Stability of the Martian Atmosphere. *Science*, *177*(4053), 986–988. https://doi.org/10.1126/science.177.4053.986

McElroy, Michael B., Yung, Y. L., & Nier, A. O. (1976). Isotopic Composition of Nitrogen: Implications for the Past History of Mars' Atmosphere. *Science*, *194*(4260), 70–72. https://doi.org/10.1126/science.194.4260.70

773 Montmessin, F., Bertaux, J.-L., Quémerais, E., Korablev, O., Rannou, P., Forget, F., et al.
774 (2006). Subvisible CO2 ice clouds detected in the mesosphere of Mars. *Icarus*,
775 *183*(2), 403–410. https://doi.org/10.1016/j.icarus.2006.03.015
776 Murchie, S. L., Mustard, J. F., Ehlmann, B. L., Milliken, R. E., Bishop, J. L., McKeown, N.
777 K., et al. (2009). A synthesis of Martian aqueous mineralogy after 1 Mars year of
778 observations from the Mars Reconnaissance Orbiter. *Journal of Geophysical*
779 *Research*, *114*, E00D06. https://doi.org/10.1029/2009JE003342
780 Olsen, K. S., Lefèvre, F., Montmessin, F., Fedorova, A. A., Trokhimovskiy, A., Baggio, L.,
781 et al. (2021). The vertical structure of CO in the Martian atmosphere from the
782 ExoMars Trace Gas Orbiter. *Nature Geoscience*, *14*, 67–71.
783 https://doi.org/10.1038/s41561-020-00678-w
784 Owen, T. (1982). The composition of the martian atmosphere. *Advances in Space Research*,
785 *2*(2), 75–80. https://doi.org/10.1016/0273-1177(82)90107-7
786 Owen, Tobias, Maillard, J. P., de Bergh, C., & Lutz, B. L. (1988). Deuterium on Mars: The
787 Abundance of HDO and the Value of D/H. *Science*, *240*(4860), 1767–1767.
788 https://doi.org/10.1126/science.240.4860.1767
789 Parkinson, T. D., & Hunten, D. M. (1972). Spectroscopy and Acronomy of O2 on Mars.
790 *Journal of the Atmospheric Sciences*, *29*(7), 1380–1390. https://doi.org/10.1175/1520-
791 0469(1972)029<1380:SAAOOO>2.0.CO;2
792 Parkinson, W. H., Rufus, J., & Yoshino, K. (2003). Absolute absorption cross section
793 measurements of in the wavelength region 163–200 nm and the temperature
794 dependence. *Chemical Physics*, *290*(2–3), 251–256. https://doi.org/10.1016/S0301-
795 0104(03)00146-0
796 Quémerais, E., Bertaux, J.-L., Korablev, O., Dimarellis, E., Cot, C., Sandel, B. R., & Fussen,
797 D. (2006). Stellar occultations observed by SPICAM on Mars Express. *Journal of*
798 *Geophysical Research*, *111*(E9), E09S04. https://doi.org/10.1029/2005JE002604
799 Scheller, E. L., Ehlmann, B. L., Hu, R., Adams, D. J., & Yung, Y. L. (2021). Long-term
800 drying of Mars by sequestration of ocean-scale volumes of water in the crust. *Science*,
801 eabc7717. https://doi.org/10.1126/science.abc7717
802 Schmidt, J. A., Johnson, M. S., & Schinke, R. (2013). Carbon dioxide photolysis from 150 to
803 210 nm: Singlet and triplet channel dynamics, UV-spectrum, and isotope effects.
804 *Proceedings of the National Academy of Sciences*, *110*(44), 17691–17696.
805 https://doi.org/10.1073/pnas.1213083110
806 Stark, G., Yoshino, K., Smith, P. L., & Ito, K. (2007). Photoabsorption cross section
807 measurements of CO2 between 106.1 and 118.7nm at 295 and 195K. *Journal of*
808 *Quantitative Spectroscopy and Radiative Transfer*, *103*(1), 67–73.
809 https://doi.org/10.1016/j.jqsrt.2006.07.001
810 Stevens, C. M., Kaplan, L., Gorse, R., Durkee, S., Compton, M., Cohen, S., & Bielling, K.
811 (1980). The kinetic isotope effect for carbon and oxygen in the reaction CO + OH.
812 *International Journal of Chemical Kinetics*, *12*(12), 935–948.
813 https://doi.org/10.1002/kin.550121205
814 Verwer, J. G., Spee, E. J., Blom, J. G., & Hundsdorfer, W. (1999). A Second-Order
815 Rosenbrock Method Applied to Photochemical Dispersion Problems. *SIAM Journal*
816 *on Scientific Computing*, *20*(4), 1456–1480.
817 https://doi.org/10.1137/S1064827597326651
818 Webster, C. R., Mahaffy, P. R., Flesch, G. J., Niles, P. B., Jones, J. H., Leshin, L. A., et al.
819 (2013). Isotope Ratios of H, C, and O in CO2 and H2O of the Martian Atmosphere.
820 *Science*, *341*(6143), 260–263. https://doi.org/10.1126/science.1237961
821 Yoshino, K., Esmond, J. R., Sun, Y., Parkinson, W. H., Ito, K., & Matsui, T. (1996).
822 Absorption cross section measurements of carbon dioxide in the wavelength region

118.7–175.5 nm and the temperature dependence. *Journal of Quantitative Spectroscopy and Radiative Transfer*, *55*(1), 53–60. https://doi.org/10.1016/0022-4073(95)00135-2

Yung, Y. L., Wen, J.-S., Pinto, J. P., Allen, M., Pierce, K. K., & Paulson, S. (1988). HDO in the Martian atmosphere: Implications for the abundance of crustal water. *Icarus*, *76*(1), 146–159. https://doi.org/10.1016/0019-1035(88)90147-9

4. Acknowledgments

The ExoMars mission is a joint mission of the European Space Agency (ESA) and Roscosmos. The ACS experiment is led by the Space Research Institute (IKI) in Moscow, assisted by LATMOS in France. This work was funded by Roscosmos, the National Centre for Space Studies of France (CNES), the Ministry of Science and Education of Russia and the UK Space Agency (ST/V002295/1 and ST/V005332/1). Science operations are funded by Roscosmos and ESA.